

000
001
002054
055
056

Multi-channel Weighted Nuclear Norm Minimization for Real Color Image Denoising

057
058
059003
004
005
006
007060
061
062
063

Anonymous ICCV submission

008
009
010
011
012064
065
066
067
068

Paper ID 572

013
014
015069
070
071

Abstract

016
017
018
019
020
021
022
023
024
025
026
027
028
029
030
031
032
033
034
035
036
037072
073
074
075
076
077
078
079
080
081
082
083
084
085
086
087
088
089
090
091
092
093
094
095
096
097
098
099
100
101
102
103
104
105
106
107

The noise structures among the R, G, B channels of real images are quite different due to the preprocessing steps in digital camera pipelines. This makes the real image denoising problem much more complex than traditional grayscale image denoising. In this paper, we propose a multi-channel optimization model for real color image denoising. Specifically, we introduce a weighting matrix into the data term to process adaptively each part of R, G, B channels in the joint patches concatenated by corresponding patches in these channels. In the regularization term, we employ the weighted nuclear norm to exploit the non-local self similar property. The proposed multi-channel weighted nuclear norm minimization (MC-WNNM) model is much more complex than the standard WNNM model. To solve this new problem, we reformulate the MC-WNNM model into a linear equality-constrained problem and solve it under the alternating direction method of multipliers (ADMM) framework. Each alternative updating step has closed-form solution and the convergence results are given. Experiments on benchmark datasets demonstrate that the proposed model outperforms state-of-the-art denoising methods on synthetic as well as real-world noisy images.

038
039
040

1. Introduction

041
042
043
044
045
046
047
048
049
050
051
052
053

Image denoising is an important problem in enhancing the image quality in computer vision systems. The traditional grayscale image denoising problem aims to recover the clean image \mathbf{x} from the noisy observation $\mathbf{y} = \mathbf{x} + \mathbf{n}$, where \mathbf{n} is often assumed to be additive white Gaussian noise (AWGN). Most image denoising methods in this field either employ the non-local self similarity (NSS) of natural images [1–7] or learn generative or discriminative denoisers from paired natural clean images and synthetic noisy images [8–12]. Among these methods, the weighted nuclear norm minimization (WNNM) method achieves excellent denoising performance by exploiting the NSS property

via low rank regularization.

The real color image denoising problem is not a trivial extension from single channel (grayscale image) to multiple channels (color image). The reason is that the noise in standard RGB (sRGB) space, though could be modeled as AWGN, are with different variances for different channels [13] due to the on-board processing steps in digital camera pipelines [14, 15]. This makes the real color image denoising problem much more complex. Directly applying the denoising methods for grayscale images to each channel of color images separately would obtain bad performance [16]. There are several work [14, 16–20] proposed specifically for color image denoising. The method [17] first transforms the color images into the luminance/chrominance space such as YCbCr before denoising, but this would make the noise distribution more complex in color images. The methods of [16, 20] process the joint patches concatenated by the corresponding patches in R, G, B channels and treat equally the patches in different channels. This would generate false colors or artifacts [16]. The methods of [14, 18, 19] ignore the non-local self similarity property of natural images, and their performance would be largely depressed [2, 7].

In order to deal with the R, G, B channels in color images more effectively, different noise properties of different channels should be considered in solving real color image denoising problem. Besides, due to its expressive denoising performance, the WNNM model [7] is employed to exploit the NSS property of natural images. In this paper, we proposed a multi-channel WNNM (MC-WNNM) model for real color image denoising. By introducing a weighting matrix to the WNNM model, the proposed MC-WNNM model no longer has closed-form solutions and more challenging to solve. By reformulating the proposed MC-WNNM model into a linear equality-constrained program with two variables, the relaxed problem can be solved under the alternating direction method of multipliers (ADMM) [21] framework. Each variable can be updated with closed-form solution [7, 22]. We also give the convergence results with detailed proof to guarantee a rational termination of the proposed algorithm.

108
109
110
111
112
113
114

2. Related Work

2.1. Weighted Nuclear Norm Minimization

As an extension to the nuclear norm minimization (NNM) model [23], the weighted nuclear norm minimization (WNNM) model [7] is described as

$$\min_{\mathbf{X}} \|\mathbf{Y} - \mathbf{X}\|_F^2 + \|\mathbf{X}\|_{\mathbf{w},*} \quad (1)$$

where $\|\mathbf{X}\|_{\mathbf{w},*} = \sum_i w_i \sigma_i(\mathbf{X})$ is the weighted nuclear norm of matrix \mathbf{X} , and $\mathbf{w} = [w_1, \dots, w_n]^\top$, $w_i \geq 0$ is the weight vector, $\sigma_i(\mathbf{X})$ is the i -th singular value of matrix \mathbf{X} . According to the Corollary 1 of [24], the problem (1) has closed-form solution if the weights are non-decreasing

$$\hat{\mathbf{X}} = \mathbf{U} \mathcal{S}_{\mathbf{w}/2}(\Sigma) \mathbf{V}^\top \quad (2)$$

where $\mathbf{Y} = \mathbf{U} \Sigma \mathbf{V}^\top$ is the singular value decomposition [25] of \mathbf{Y} and $\mathcal{S}_\tau(\bullet)$ is the generalized soft-thresholding operator with weight vector \mathbf{w} :

$$\mathcal{S}_{\mathbf{w}/2}(\Sigma_{ii}) = \max(\Sigma_{ii} - w_{ii}/2, 0) \quad (3)$$

Though having achieved excellent performance on grayscale image denoising, the WNNM model would generate false colors or artifacts [16], if being directly extended to real color image denoising by processing each channel separately or joint vectors concatenated by multiple channels. In this paper, for real noisy image denoising, we propose a multi-channel WNNM model which preserve the power of WNNM and be able to process the differences among different channels.

2.2. Real Color Image Denoising

During the last decade, several denoising methods are proposed for real color image denoising [17–20]. Among them, the CBM3D [17] first transform the RGB image into luminance-chrominance space (e.g., YCbCr) and then apply the famous BM3D method [2] on each channel separately with the patches being grouped only in the luminance channel. In [18], the authors proposed the “Noise Level Function” to estimate and remove the noise for each channel in natural images. However, the methods processing each channel separately would achieve inferior performance than processing jointly these channels [16]. The methods of [19, 20, 26] perform real color image denoising by concatenating the patches in R, G, B channels into joint vectors. However, the concatenation would treat each channel equally and ignore the different noise properties among these channels. The method in [14] models the cross-channel noise in real noisy image as a multivariate Gaussian and the noise is removed by the Bayesian nonlocal means filter [27]. The commercial software Neat Image [28] estimates the noise parameters from a flat region of the given noisy image and filters the noise correspondingly. But

these methods [14, 28] ignore the non-local self similarity property of natural images [2, 7].

In this paper, we introduce a weighting matrix which add different weights to different channels for color image denoising. The proposed multi-channel method can effectively solve the problem of different noise structures among different channels.

3. Color Image Denoising via Multi-channel Weighted Nuclear Norm Minimization

3.1. The Problem

The color image denoising problem is to recover the clean image \mathbf{x}_c from its noisy version $\mathbf{y}_c = \mathbf{x}_c + \mathbf{n}_c$, where $c = \{r, g, b\}$ is the index of R, G, B channels and \mathbf{n}_c is the noise in c -th channel. Given a noisy color image \mathbf{y}_c , each local patch of size $p \times p \times 3$ is extracted and stretched to a patch vector $\mathbf{y} = [\mathbf{y}_r^\top \mathbf{y}_g^\top \mathbf{y}_b^\top]^\top \in \mathbb{R}^{3p^2}$, where $\mathbf{y}_r, \mathbf{y}_g, \mathbf{y}_b \in \mathbb{R}^{p^2}$ are corresponding patches in R, G, B, channels. For each local patch \mathbf{y} , we search the M most similar patches to it (including \mathbf{y} itself) by Euclidean distance in a $W \times W$ local region around it. We stack the M similar patches column by column to form a noisy patch matrix $\mathbf{Y} = \mathbf{X} + \mathbf{N} \in \mathbb{R}^{3p^2 \times M}$, where \mathbf{X} and \mathbf{N} the corresponding clean and noise patch matrices.

According to [13], the noise in standard RGB (sRGB) space though could be modeled as additive white Gaussian (AWGN) with different variances for different channels. Therefore, it is problematic to directly apply denoising methods to the joint vectors concatenated by corresponding patches of the R, G, B channels. To validate this point, in Fig. 1, we show the clean image ‘‘kodim23’’ taken from the Kodak PhotoCD dataset, its degraded version generated by adding synthetic additive white Gaussian noise (AWGN) to each channel of ‘‘kodim23’’, and the denoised image by applying WNNM [7] on the joint vectors concatenated from R, G, B channels of the degraded image. The standard derivations of AWGN added to the R, G, B channels are $\sigma_r = 40$, $\sigma_g = 20$, $\sigma_b = 30$, respectively. The input standard derivation of the noise for the concatenated WNNM method is set as the Root Mean Square (RMS) of those in each channel, i.e., $\sigma = \sqrt{(\sigma_r^2 + \sigma_g^2 + \sigma_b^2)/3} = 31.1$. From Fig. 1, one can see that the concatenated WNNM method treating each channel equally would remain some noise in the R and B channel, while over-smoothing the G channel of the degraded image. Hence, if the patches of different channels are treated adaptively in the concatenated vectors, the degraded color images would be recovered with better visual qualities.

In order to process each channel differently while still exploiting the joint structures of the color images, in this paper, we introduce a weighting matrix \mathbf{W} to the concatenated

162
163
164
165
166
167
168
169
170
171
172
173
174
175
176
177
178
179
180
181
182
183
184
185
186
187
188
189
190
191
192
193
194
195
196
197
198
199
200
201
202
203
204
205
206
207
208
209
210
211
212
213
214
215

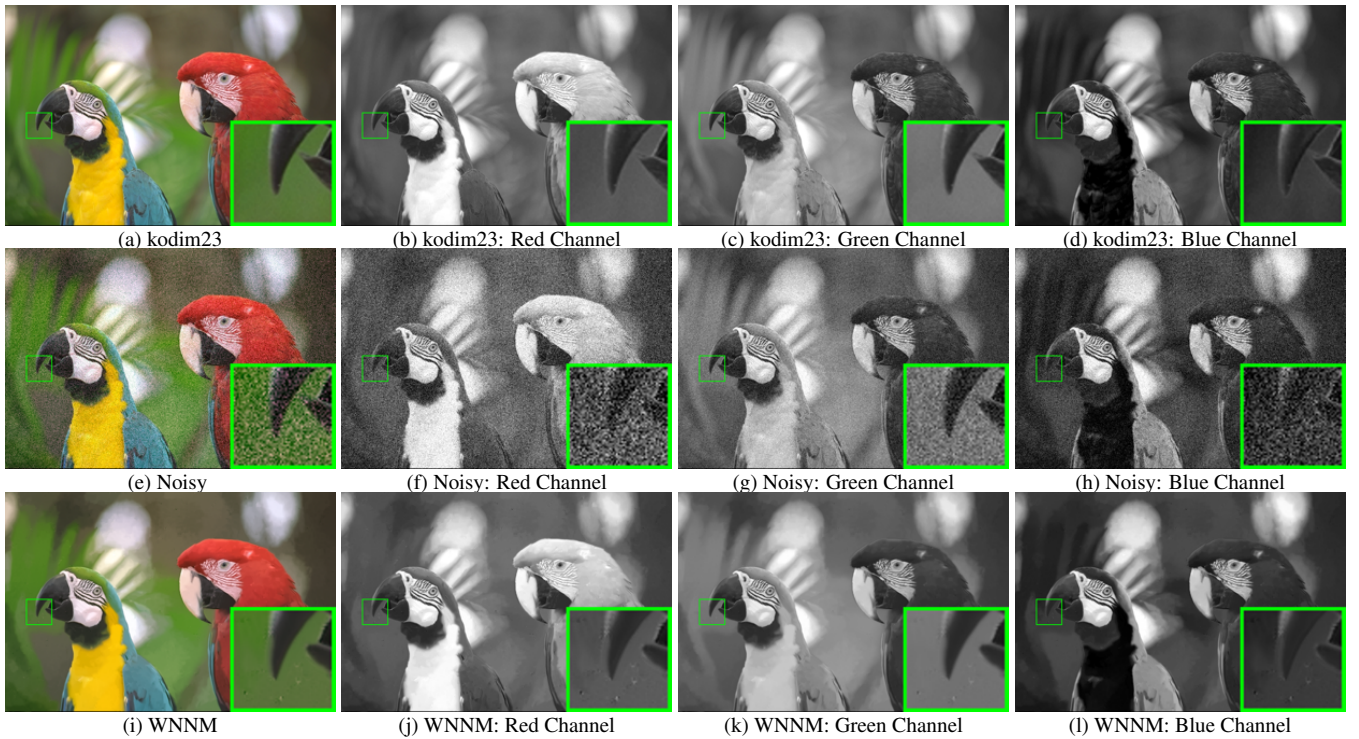


Figure 1. The image “kodim23” of the Kodak PhotoCD dataset, its degraded version, and the image recovered by WNNM. The R, G, B channels are also listed here for image quality comparison.

WNNM method. The weights \mathbf{w} for the singular values of \mathbf{X} , then the proposed multi-channel WNNM (MC-WNNM) model is

$$\min_{\mathbf{X}} \|\mathbf{W}(\mathbf{Y} - \mathbf{X})\|_F^2 + \|\mathbf{X}\|_{\mathbf{w},*}. \quad (4)$$

How to set the weighting matrix \mathbf{W} and how to solve the proposed model will be introduced in the next sections.

3.2. The Setting of Weighting Matrix \mathbf{W}

For simplicity, in this paper, we assume the noise are independent among the R, G, B channels and i.i.d. in each channel. Assume the noisy patch matrix $\mathbf{Y} = [\mathbf{Y}_r^\top \mathbf{Y}_g^\top \mathbf{Y}_b^\top]^\top$, where $\mathbf{Y}_r, \mathbf{Y}_g, \mathbf{Y}_b$ are matrices of similar patches in R, G, B channels, respectively. The corresponding clean matrix $\mathbf{X} = [\mathbf{X}_r^\top \mathbf{X}_g^\top \mathbf{X}_b^\top]^\top$, where $\mathbf{X}_r, \mathbf{X}_g, \mathbf{X}_b$ are similarly defined. Therefore, the weighting matrix \mathbf{W} is diagonal and can be determined under the Bayesian framework:

$$\begin{aligned} \hat{\mathbf{X}} &= \arg \max_{\mathbf{X}} \ln P(\mathbf{X} | \mathbf{Y}, \mathbf{w}) \\ &= \arg \max_{\mathbf{X}} \{\ln P(\mathbf{Y} | \mathbf{X}) + \ln P(\mathbf{X} | \mathbf{w})\}. \end{aligned} \quad (5)$$

The log-likelihood term $\ln P(\mathbf{Y} | \mathbf{X})$ is characterized by the statistics of noise, which is assumed to be channel-wise independent white Gaussian with standard deviations $\{\sigma_r, \sigma_g, \sigma_b\}$

$$P(\mathbf{Y} | \mathbf{X}) = \prod_{c \in \{r,g,b\}} (2\pi\sigma_c^2)^{-\frac{3p^2}{2}} \exp\left(-\frac{1}{2\sigma_c^2} \|\mathbf{Y}_c - \mathbf{X}_c\|_F^2\right). \quad (6)$$

We assume that the matrix \mathbf{X} follows the following distribution

$$P(\mathbf{X} | \mathbf{w}) \propto \exp\left(-\frac{1}{2} \|\mathbf{X}\|_{\mathbf{w},*}\right). \quad (7)$$

Putting (7) and (6) into (5), we have

$$\begin{aligned} \hat{\mathbf{X}} &= \arg \min_{\mathbf{X}} \sum_{c \in \{r,g,b\}} \frac{1}{\sigma_c^2} \|(\mathbf{Y}_c - \mathbf{X}_c)\|_F^2 + \|\mathbf{X}\|_{\mathbf{w},*} \\ &= \arg \min_{\mathbf{X}} \|\mathbf{W}(\mathbf{Y} - \mathbf{X})\|_F^2 + \|\mathbf{X}\|_{\mathbf{w},*}, \end{aligned} \quad (8)$$

where

$$\mathbf{W} = \begin{pmatrix} \sigma_r^{-1} \mathbf{I} & \mathbf{0} & \mathbf{0} \\ \mathbf{0} & \sigma_g^{-1} \mathbf{I} & \mathbf{0} \\ \mathbf{0} & \mathbf{0} & \sigma_b^{-1} \mathbf{I} \end{pmatrix}. \quad (9)$$

where $\mathbf{I} \in \mathbb{R}^{p^2 \times p^2}$ is the identity matrix. Hence, the weighting matrix \mathbf{W} is determined to contribute equal weights for the pixel values in the same channel, while different weights for those in different channels. The experimental (which will be introduced later) results have already demonstrated that this form of weighting matrix have already generated the best denoising performance on synthetic and real noisy images in benchmark datasets.

324
 325 **Algorithm 1:** Color Image Denoising by MC-WNNM
 326 **Input:** Noisy image \mathbf{y} , noise levels $\{\sigma_r, \sigma_g, \sigma_b\}$;
 327 **Initialization:** $\hat{\mathbf{x}}^{(0)} = \mathbf{y}, \mathbf{y}^{(0)} = \mathbf{y}$;
 328 **for** $k = 1 : K_1$ **do**
 329 1. Set $\mathbf{y}^{(k)} = \hat{\mathbf{x}}^{(k-1)}$;
 330 2. Extract local patches $\{\mathbf{y}_j\}_{j=1}^N$ from $\mathbf{y}^{(k)}$;
 331 **for each patch** \mathbf{y}_j **do**
 332 3. Search non-local similar patches \mathbf{Y}_j ;
 333 4. Apply the MC-WNNM model (10) to \mathbf{Y}_j and
 334 obtain the estimated \mathbf{X}_j ;
 335 **end for**
 336 5. Aggregate $\{\mathbf{X}_j\}_{j=1}^N$ to form the image $\hat{\mathbf{x}}^{(k)}$;
 337 **end for**
 338 **Output:** Denoised image $\hat{\mathbf{x}}^{K_1}$.

3.3. The Denoising Algorithm

Then, we can apply the proposed MC-WNNM model to \mathbf{Y}_j to estimate \mathbf{X}_j for color image denoising:

$$\min_{\mathbf{X}_j} \|\mathbf{W}_j(\mathbf{Y}_j - \mathbf{X}_j)\|_F^2 + \|\mathbf{X}_j\|_{w,*}. \quad (10)$$

where \mathbf{W}_j is defined in Eq. (9). Just as [24] did, the weight vector w is set $w_i^{k+1} = \frac{C}{|\sigma_i(\mathbf{X}_k)| + \epsilon}$ and $\epsilon > 0$ is a small number to avoid zero numerator. Note that when $\sigma_r = \sigma_g = \sigma_b$, the multi-channel WNNM model will be reduced to the concatenated WNNM model as a special case.

The multi-channel WNNM is applied to the noisy patch matrix \mathbf{Y}_j of each local patch \mathbf{y}_j in the noisy image \mathbf{y} . And then all the patches are aggregated together to form the final recovered image $\hat{\mathbf{y}}$. To obtain better denoising results, we perform the above denoising procedure for several (K_1) iterations. The proposed MC-WNNM denoising algorithm for color images is summarized in Algorithm 1.

3.4. Optimization

The proposed MC-WNNM model could not be solved in an analytical form while the original WNNM model [24] could. In the WNNM model, when the weights on singular values are non-descending, the weighted nuclear norm proximal operator [24] can have global optimum with closed-form solution. However, such property is not valid for the multi-channel WNNM model. The reason is that the weighting matrix \mathbf{W} is added to the rows of matrix \mathbf{X} instead of its singular values. Besides, the elements in \mathbf{W} is not in a non-descending order with respect to the singular value of \mathbf{X} . This makes the proposed model more difficult to solve when compared to the original WNNM model.

By introducing an augmented variable \mathbf{Z} , the MC-WNNM model is reformulated as a linear equality-constrained problem with two variables \mathbf{X} and \mathbf{Z} :

$$\min_{\mathbf{X}, \mathbf{Z}} \|\mathbf{W}(\mathbf{Y} - \mathbf{X})\|_F^2 + \|\mathbf{Z}\|_{w,*} \quad \text{s.t. } \mathbf{X} = \mathbf{Z}. \quad (11)$$

Since the objective function is separable across the two variables, the problem (11) can be solved under alternating direction method of multipliers (ADMM) framework. We can derive its augmented Lagrangian function:

$$\begin{aligned} \mathcal{L}(\mathbf{X}, \mathbf{Z}, \mathbf{A}, \rho) = & \|\mathbf{W}(\mathbf{Y} - \mathbf{X})\|_F^2 + \|\mathbf{Z}\|_{w,*} \\ & + \langle \mathbf{A}, \mathbf{X} - \mathbf{Z} \rangle + \frac{\rho}{2} \|\mathbf{X} - \mathbf{Z}\|_F^2 \end{aligned} \quad (12)$$

where \mathbf{A} is the augmented Lagrangian multiplier and $\rho > 0$ is the penalty parameter. We initialize the matrix variables \mathbf{X}_0 , \mathbf{Z}_0 , and \mathbf{A}_0 to be zero matrix of suitable size. By taking derivative of the Lagrangian function \mathcal{L} with respect to the variables \mathbf{X} and \mathbf{Z} and setting the derivative function to be zero, we can alternatively update the ADMM algorithm iteratively as follows:

(1) **Update \mathbf{X} while fixing \mathbf{Z} and \mathbf{A} :**

$$\mathbf{X}_{k+1} = \arg \min_{\mathbf{X}} \|\mathbf{W}(\mathbf{Y} - \mathbf{X})\|_F^2 + \frac{\rho_k}{2} \|\mathbf{X} - \mathbf{Z}_k + \rho_k^{-1} \mathbf{A}_k\|_F^2 \quad (13)$$

This is a standard least squares regression problem with closed-form solution:

$$\mathbf{X}_{k+1} = (\mathbf{W}^\top \mathbf{W} + \frac{\rho_k}{2} \mathbf{I})^{-1} (\mathbf{W}^\top \mathbf{W} \mathbf{Y} + \frac{\rho_k}{2} \mathbf{Z}_k - \frac{1}{2} \mathbf{A}_k) \quad (14)$$

(2) **Update \mathbf{Z} while fixing \mathbf{X} and \mathbf{A} :**

$$\mathbf{Z}_{k+1} = \arg \min_{\mathbf{Z}} \frac{\rho_k}{2} \|\mathbf{Z} - (\mathbf{X}_{k+1} + \rho_k^{-1} \mathbf{A}_k)\|_F^2 + \|\mathbf{Z}\|_{w,*} \quad (15)$$

According to the Theorem 1 in [24], given the $\mathbf{X}_{k+1} + \rho_k^{-1} \mathbf{A}_k = \mathbf{U}_k \boldsymbol{\Sigma}_k \mathbf{V}_k^\top$ be the SVD of $\mathbf{X}_{k+1} + \rho_k^{-1} \mathbf{A}_k$, where $\boldsymbol{\Sigma}_k = \begin{pmatrix} \text{diag}(\sigma_1, \sigma_2, \dots, \sigma_n) \\ \mathbf{0} \end{pmatrix} \in \mathbb{R}^{m \times n}$, then the global optimum of the above problem is $\hat{\mathbf{Z}} = \mathbf{U}_k \hat{\boldsymbol{\Sigma}}_k \mathbf{V}_k^\top$, where $\hat{\boldsymbol{\Sigma}}_k = \begin{pmatrix} \text{diag}(\hat{\sigma}_1, \hat{\sigma}_2, \dots, \hat{\sigma}_n) \\ \mathbf{0} \end{pmatrix} \in \mathbb{R}^{m \times n}$ and $(\hat{\sigma}_1, \hat{\sigma}_2, \dots, \hat{\sigma}_n)$ is the solution to the following convex optimization problem:

$$\begin{aligned} \min_{\hat{\sigma}_1, \hat{\sigma}_2, \dots, \hat{\sigma}_n} & \sum_{i=1}^n (\sigma_i - \hat{\sigma}_i)^2 + \frac{2w_i}{\rho_k} \hat{\sigma}_i \\ \text{s.t. } & \hat{\sigma}_1 \geq \hat{\sigma}_2 \geq \dots \geq \hat{\sigma}_n \geq 0. \end{aligned} \quad (16)$$

According to the Remark 1 in [24], the problem above has closed-form solution

$$\hat{\sigma}_i = \begin{cases} 0 & \text{if } c_2 < 0 \\ \frac{c_1 + \sqrt{c_2}}{2} & \text{if } c_2 \geq 0 \end{cases} \quad (17)$$

where $c_1 = \sigma_i - \epsilon$, $c_2 = (\sigma_i - \epsilon)^2 - \frac{8C}{\rho_k}$ and C is set as $\sqrt{2n}$ by experience in image denoising.

(3) **Update \mathbf{A} while fixing \mathbf{X} and \mathbf{Z} :**

$$\mathbf{A}_{k+1} = \mathbf{A}_k + \rho_k (\mathbf{X}_{k+1} - \mathbf{Z}_{k+1}) \quad (18)$$

(4) **Update ρ_k :** $\rho_{k+1} = \mu * \rho_k$, where $\mu > 1$.

Algorithm 2: Solve MC-WNNM via ADMM

```

Input: Matrices  $\mathbf{Y}$  and  $\mathbf{W}$ ,  $\mu > 1$ , Tol > 0;
Initialization:  $\mathbf{X}_0 = \mathbf{Z}_0 = \mathbf{A}_0 = \mathbf{0}$ ,  $\rho_0 > 0$ , T = False,
 $k = 0$ ;
While (T == false) do
    1. Update  $\mathbf{X}_{k+1}$  as
     $\mathbf{X}_{k+1} = (\mathbf{W}^\top \mathbf{W} + \frac{\rho_k}{2} \mathbf{I})^{-1} (\mathbf{W}^\top \mathbf{W} \mathbf{Y} + \frac{\rho_k}{2} \mathbf{Z}_k - \frac{1}{2} \mathbf{A}_k)$ 
    2. Update  $\mathbf{Z}_{k+1}$  by solving the problem
         $\min_{\mathbf{Z}} \frac{\rho_k}{2} \|\mathbf{Z} - (\mathbf{X}_{k+1} + \rho_k^{-1} \mathbf{A}_k)\|_F^2 + \|\mathbf{Z}\|_{w,*}$ 
    3. Update  $\mathbf{A}_{k+1}$  as  $\mathbf{A}_{k+1} = \mathbf{A}_k + \rho_k (\mathbf{X}_{k+1} - \mathbf{Z}_{k+1})$ 
    4. Update  $\rho_{k+1} = \mu * \rho_k$ ;
    5.  $k \leftarrow k + 1$ ;
        if (Convergence conditions are satisfied) or ( $k \geq K_2$ )
    5. T  $\leftarrow$  True
        end if
end while
Output: Matrices  $\mathbf{X}$  and  $\mathbf{Z}$ .

```

The above alternative updating steps are repeated until the convergence condition is satisfied or the number of iterations exceeds a preset maximum number, e.g., K_2 . The convergence condition of the ADMM algorithm is: $\|\mathbf{X}_{k+1} - \mathbf{Z}_{k+1}\|_F \leq \text{Tol}$, $\|\mathbf{X}_{k+1} - \mathbf{X}_k\|_F \leq \text{Tol}$, and $\|\mathbf{Z}_{k+1} - \mathbf{Z}_k\|_F \leq \text{Tol}$ are simultaneously satisfied, where $\text{Tol} > 0$ is a small tolerance. We summarize the updating steps in Algorithm 2. The convergence analysis of the proposed Algorithm 2 is given in Theorem 1. Note that since the weighted nuclear norm is non-convex in general, we employ an unbounded sequence of $\{\rho_k\}$ here to make sure that the Algorithm 2 is convergent.

Theorem 1. Assume the weights in w are in a non-descending order; the sequence $\{\mathbf{X}_k\}$, $\{\mathbf{Z}_k\}$, and $\{\mathbf{A}_k\}$ generated in Algorithm 1 satisfy:

$$(a) \lim_{k \rightarrow \infty} \|\mathbf{X}_{k+1} - \mathbf{Z}_{k+1}\|_F = 0; \quad (19)$$

$$(b) \lim_{k \rightarrow \infty} \|\mathbf{X}_{k+1} - \mathbf{X}_k\|_F = 0; \quad (20)$$

$$(c) \lim_{k \rightarrow \infty} \|\mathbf{Z}_{k+1} - \mathbf{Z}_k\|_F = 0. \quad (21)$$

Proof. We give proof sketch here and detailed proof of this theorem can be found in supplementary files. We can first proof that the sequence $\{\mathbf{A}_k\}$ generated by Algorithm 3.4 is upper bounded. Since $\{\rho_k\}$ is unbounded, that is $\lim_{k \rightarrow \infty} \rho_k = +\infty$, we can proof that the sequence of Lagrangian function $\{\mathcal{L}(\mathbf{X}_{k+1}, \mathbf{Z}_{k+1}, \mathbf{A}_k, \rho_k)\}$ is also upper bounded. Hence, both $\{\mathbf{W}(\mathbf{Y} - \mathbf{X}_k)\}$ and $\{\mathbf{Z}_k\}$ are upper bounded. According to Eq. (18), we can proof that $\lim_{k \rightarrow \infty} \|\mathbf{X}_{k+1} - \mathbf{Z}_{k+1}\|_F = \lim_{k \rightarrow \infty} \rho_k^{-1} \|\mathbf{A}_{k+1} - \mathbf{A}_k\|_F = 0$, and (a) is proofed. Then we can proof that $\lim_{k \rightarrow \infty} \|\mathbf{X}_{k+1} - \mathbf{X}_k\|_F \leq \lim_{k \rightarrow \infty} \|(\mathbf{W}^\top \mathbf{W} + \frac{\rho_k}{2} \mathbf{I})^{-1} (\mathbf{W}^\top \mathbf{W} \mathbf{Y} - \mathbf{W}^\top \mathbf{W} \mathbf{Z}_k - \frac{1}{2} \mathbf{A}_k)\|_F + \rho_k^{-1} \|\mathbf{A}_k - \mathbf{A}_{k-1}\|_F = 0$ and hence (b) is proofed. Then (c) can

be proved by checking that $\lim_{k \rightarrow \infty} \|\mathbf{Z}_{k+1} - \mathbf{Z}_k\| \leq \lim_{k \rightarrow \infty} \|\Sigma_{k-1} - \mathcal{S}_{w/\rho_{k-1}}(\Sigma_{k-1})\|_F + \|\mathbf{X}_{k+1} - \mathbf{X}_k\|_F + \rho_k^{-1} \|\mathbf{A}_{k-1} + \mathbf{A}_{k+1} - \mathbf{A}_k\|_F = 0$, where $\mathbf{U}_{k-1} \Sigma_{k-1} \mathbf{V}_{k-1}^\top$ is the SVD of the matrix $\mathbf{X}_k + \rho_{k-1} \mathbf{A}_{k-1}$. \square

4. Experiments

We evaluate the proposed MC-WNNM method on synthetic and real color image denoising. We compare the proposed method with other state-of-the-art denoising methods including CBM3D [17], MLP [10], WNNM [7], TNRD [12], “Noise Clinic” (NC) [19, 26], and the commercial software Neat Image (NI) [28].

4.1. Implementation Details

In synthetic experiments, the noise levels in R, G, B channels are assumed to be known as $\sigma_r, \sigma_g, \sigma_b$. In the real cases, the noise levels in R, G, B channels can be estimated via noise estimation methods [29, 30]. In this paper, we employ the method of [30] for its state-of-the-art performance. For the CBM3D method [17], the input noise levels are the Root Mean Square (RMS) as

$$\sigma = \sqrt{(\sigma_r^2 + \sigma_g^2 + \sigma_b^2)/3}. \quad (22)$$

For the methods of MLP [10] and TNRD [12], we retrain the models on grayscale images following their corresponding strategies at different noise levels from $\sigma = 5$ to $\sigma = 75$ with gap of 5. The denoising on color images is performed by processing separately each channel with the model trained at the same (or nearest) noise levels. NC [19, 26] is a blind image denoising method, so we just submit the noisy images (synthetic or real) to [26] and perform denoising using the default parameters. NI [28] is a commercial software suitable for real image denoising, while the code of CC [14] is not released (but its results on the 15 real noisy images in [14] are available by requesting the authors). Hence, we only compare with CC and NI in real image denoising experiments, and do not compare with them in synthetic experiments.

In order to take fully comparison with the original WNNM method [24], we extended the WNNM method [24] for color image denoising in three directions: 1) we apply the WNNM method [24] on each channel separately with corresponding noise levels $\sigma_r, \sigma_g, \sigma_b$. We call this method “WNNM0”; 2) we perform denoising on the joint vectors concatenated by corresponding patches in the R, G, B channels, where the input noise level σ is computed by RMS (Eq. (22)). We call this method “WNNM1”; 3) we set the weighting matrix \mathbf{W} in the proposed MC-WNNM model as $\mathbf{W} = \sigma^{-1}\mathbf{I}$. For fair comparison, we tune all these methods set the same parameters for “WNNM2” and the proposed MC-WNNM methods while achieving the best performance of “WNNM2”. For fair comparison, we tune the methods of “WNNM0”, “WNNM1”, “WNNM2”, and the proposed

540 MC-WNNM to achieve corresponding best denoising per-
 541 formance (i.e., highest average PSNR results).
 542
 543
 544

4.2. Experiments on Synthetic Noisy Images

547 In this section, we compare the proposed MC-WNNM
 548 method with other competing denoising methods [10, 12,
 549 17, 19, 28] as well as the three extensions of the original
 550 WNNM method [24] on the 24 high quality color images from
 551 the Kodak PhotoCD Dataset (<http://r0k.us/graphics/kodak/>), which are shown in Fig. 2.
 552 The noisy images are generated by adding additive white
 553 Gaussian noise (AWGN) with known standard derivations
 554 $\sigma_r, \sigma_g, \sigma_b$ for the R, G, B channels, respectively. In this
 555 paper, the noise levels we add to each channel of the 24
 556 color images are $\sigma_r = 40, \sigma_g = 20, \sigma_b = 30$, respectively.
 557 More experiments can be found in the supplementary files.
 558 For the methods of “WNNM2” and MC-WNNM, we set the
 559 patch size as $p = 6$, the number of non-local similar patches
 560 as $M = 70$, the window size for searching similar patches
 561 as $W = 20$, the updating parameter $\mu = 1.001$, the num-
 562 ber of iterations in Algorithm 1 as $K_1 = 8$, the number of
 563 iterations in Algorithm 2 as $K_2 = 10$. For “WNNM2”, the
 564 initial penalty parameter is set as $\rho_0 = 10$, while for the
 565 proposed MC-WNNM model, the penalty parameter is set
 566 as $\rho_0 = 3$.
 567

568 The PSNR results are listed in Table 1 of the com-
 569 pared methods including CBM3D [17], MLP [10], TNRD
 570 [12], NI [28], NC [19, 26], “WNNM0” [24], “WNNM1”,
 571 “WNNM2” and the proposed MC-WNNM methods. The
 572 best PSNR results are highlighted in bold. One can see that
 573 on all the 24 images, our method achieves the highest PSNR
 574 values over the competing methods. On average PSNR,
 575 our proposed method achieves 0.48dB improvements over
 576 the “WNNM0” method and outperforms the “WNNM2”
 577 by 1.09dB. Fig. 3 shows a scene denoised by the
 578 compared methods. We can see that the methods of CBM3D
 579 and NC would remain some noise on the recovered images.
 580 The methods of MLP, TNRD, and “WNNM0”, which
 581 process separately the channels of color images, would
 582 over-smooth the images and generate false colors or artifacts.
 583 The method “WNNM1”, which process jointly the chan-
 584 nels of color images, would not generate false colors, but
 585 still over-smooth the image. The “WNNM2”, which is the
 586 WNNM model solved by ADMM algorithm, would remain
 587 some noise on the image. By employing the proposed MC-
 588 WNNM model, our method preserves the structures (e.g.,
 589 textures in windows and grass) better across the R, G, B
 590 channels and generate less artifacts than other denoising
 591 methods, leading to visually pleasant outputs. More visual
 592 comparisons can be found in the supplementary files.
 593



Figure 2. The 24 high quality color images from the Kodak PhotoCD Dataset.

4.3. Experiments on Real Noisy Images

594 In this section, we compare the proposed MC-WNNM
 595 method with other competing methods on the 15 real noisy
 596 images (Fig. 4). We do not compare with the “WNNM0”
 597 method due to limited space and its inferior performance.
 598 The noisy images were collected under controlled indoor
 599 environment. Each scene was shot 500 times under the same
 600 camera and camera setting. The mean image of the 500
 601 shots is roughly taken as the “ground truth”, with which the
 602 PSNR can be computed. Since the image size is very large
 603 (about 7000×5000) and the 11 scenes share repetitive con-
 604 tents, the authors of [14] cropped 15 smaller images (of size
 605 512×512) to perform experiments. For each real noisy im-
 606 age, the noise levels in R, G, B channels are estimated by
 607 [30]. Since the noise levels are small in real noisy images,
 608 for the method of MLP [10] and TNRD [12], we apply the
 609 trained models of corresponding methods and choose the
 610 best denoising results (highest average PSNR values). Both
 611 methods achieves best results when setting the noise levels
 612 of the trained models from $\sigma = 10$.

613 We perform quantitative comparison on the 15 cropped
 614 images used in [14]. The PSNR results are listed in Ta-
 615 ble 2 of the compared methods including CBM3D [17],
 616 MLP [10], TNRD [12], NC [19, 26], NI [28], CC [14]
 617 (copied from [14]), “WNNM1”, “WNNM2”, and the pro-
 618 posed MC-WNNM method. The highest PSNR results are
 619 highlighted in bold. On average PSNR, the proposed MC-
 620 WNNM method achieves 0.44dB improvements over the
 621 “WNNM1” method and outperforms the state-of-the-art de-
 622 noising method CC [14] by 0.83dB. On 10 out of the whole
 623 15 images, the proposed MC-WNNM method achieves the
 624 highest PSNR values. Both CC and “WNNM1” achieves
 625 highest PSNR results on 2 of 15 images. It should be noted
 626 that in the CC method, a specific model is trained for each
 627 camera and camera setting, while our method uses the same
 628 model for all cases. Fig. 5 shows the denoised images of
 629 a scene captured by Canon 5D Mark 3 at ISO = 3200. We
 630 can see that CBM3D, NC, NI and CC would either remain
 631 noise or generate artifacts, while TNRD, “WNNM1”, and
 632 “WNNM2” over-smooth much the image. By using the pro-
 633

648

649

650

651

652

653

654

655

656

657

658

659

660

661

662

663

664

665

666

667

668

669

670

671

672

673

674

675

676

677

678

679

680

681

682

683

684

685

686

687

688

689

690

691

692

693

694

695

696

697

698

699

700

701

702

703

704

705

706

707

708

709

710

711

712

713

714

715

716

717

718

719

720

721

722

723

724

725

726

727

728

729

730

731

732

733

734

735

736

737

738

739

740

741

742

743

744

745

746

747

748

749

750

751

752

753

754

755

Table 1. PSNR(dB) results of different denoising algorithms on 24 natural images.

Image#	$\sigma_r = 40, \sigma_g = 20, \sigma_b = 30$								
	CBM3D	MLP	TNRD	NI	NC	WNNM0	WNNMI	WNNM2	MC-WNNM
1	25.24	25.70	25.74	23.85	24.90	26.01	25.95	25.58	26.66
2	28.27	30.12	30.21	25.90	25.87	30.08	30.11	29.80	30.20
3	28.81	31.19	31.49	26.00	28.58	31.58	31.61	31.20	32.25
4	27.95	29.88	29.86	25.82	25.67	30.13	30.16	29.84	30.49
5	25.03	26.00	26.18	24.38	25.15	26.44	26.39	25.32	26.82
6	26.24	26.84	26.90	24.65	24.74	27.39	27.30	26.88	27.98
7	27.88	30.28	30.40	25.63	27.69	30.47	30.54	29.70	30.98
8	25.05	25.59	25.83	24.02	25.30	26.71	26.75	25.26	26.90
9	28.44	30.75	30.81	25.94	27.44	30.86	30.92	30.29	31.49
10	28.27	30.38	30.57	25.87	28.42	30.65	30.68	29.95	31.26
11	26.95	28.00	28.14	25.32	24.67	28.19	28.16	27.61	28.63
12	28.76	30.87	31.05	26.01	28.37	30.97	31.06	30.58	31.48
13	23.76	23.95	23.99	23.53	22.76	24.27	24.15	23.52	24.89
14	26.02	26.97	27.11	24.94	25.68	27.20	27.15	26.55	27.57
15	28.38	30.15	30.44	26.06	28.21	30.52	30.60	30.13	30.81
16	27.75	28.82	28.87	25.69	26.66	29.27	29.21	29.02	29.96
17	27.90	29.57	29.80	25.85	28.32	29.78	29.79	29.16	30.40
18	25.77	26.40	26.41	24.74	25.70	26.63	26.56	26.01	27.22
19	27.30	28.67	28.81	25.40	26.52	29.19	29.22	28.67	29.57
20	28.96	30.40	30.76	24.95	25.90	30.79	30.83	29.97	31.07
21	26.54	27.53	27.60	25.06	26.48	27.80	27.75	27.12	28.34
22	27.05	28.17	28.27	25.36	26.60	28.21	28.16	27.81	28.64
23	29.14	32.31	32.51	26.13	23.24	31.89	31.97	31.21	32.34
24	25.75	26.41	26.53	24.55	25.73	27.10	27.03	26.18	27.59
Average	27.13	28.54	28.68	25.24	26.19	28.84	28.83	28.22	29.31

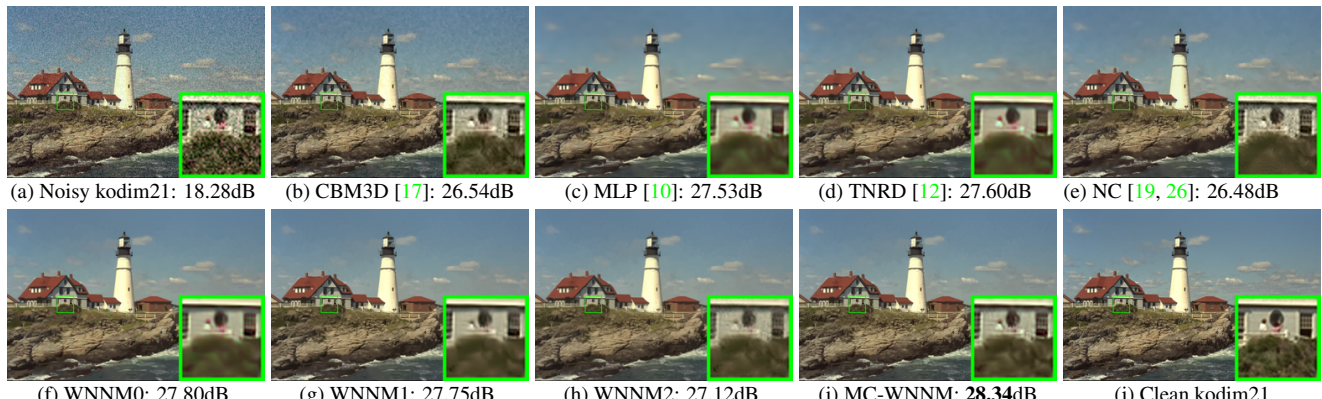
Figure 3. Denoised images of different methods on the image "kodim21" degraded by AWGN with different standard derivations of $\sigma_r = 40, \sigma_g = 20, \sigma_b = 30$ on R, G, B channels, respectively. The images are better to be zoomed in on screen.

Figure 4. The 15 cropped real noisy images used in [14].

posed MC-WNNM model achieves better visual quality results than other methods. More visual comparisons can be found in the supplementary files.

5. Conclusion and Future Work

The real noisy images have different noise structures among the R, G, B channels due to the preprocessing steps of the digital camera pipelines in CCD or CMOS sensors. This makes the real image denoising problem much more complex than grayscale image denoising. In this paper, we proposed a novel multi-channel (MC) model for real color image denoising. By introducing a weighting matrix to the concatenated weighted nuclear norm minimization (WNNM) model, the proposed MC-WNNM model can process adaptively the different noise structures in each of the R, G, B channels and exploit the non-local self similarity property of natural images. Though no longer having closed-form solution, we successfully solved the MC-WNNM model via an ADMM algorithm by reformulating the MC-WNNM model as a linear equality-constrained

Table 2. PSNR(dB) results of different methods on 15 cropped real noisy images used in [14].

Camera Settings	CBM3D	MLP	TNRD	NI	NC	CC	WNNM1	WNNM2	MC-WNNM
Canon 5D Mark III ISO = 3200	39.76 36.40 36.37	39.00 36.34 36.33	39.51 36.47 36.45	35.68 34.03 32.63	36.20 34.35 33.10	38.37 35.37 34.91	39.74 35.12 33.14	39.98 36.65 34.63	41.13 37.28 36.52
Nikon D600 ISO = 3200	34.18 35.07 37.13	34.70 36.20 39.33	34.79 36.37 39.49	31.78 35.16 39.98	32.28 35.34 40.51	34.98 35.95 41.15	35.08 36.42 40.78	35.08 36.84 39.24	35.53 37.02 39.56
Nikon D800 ISO = 1600	36.81 37.76 37.51	37.95 40.23 37.94	38.11 40.52 38.17	34.84 38.42 35.79	35.09 38.65 35.85	37.99 40.36 38.30	38.28 41.24 38.04	38.61 40.81 38.96	39.26 41.43 39.55
Nikon D800 ISO = 3200	35.05 34.07 34.42	37.55 35.91 38.15	37.69 35.90 38.21	38.36 35.53 40.05	38.56 35.76 40.59	39.01 36.75 39.06	39.93 37.32 41.52	37.97 37.30 38.68	38.91 37.41 39.39
Nikon D800 ISO = 6400	31.13 31.22 30.97	32.69 32.33 32.29	32.81 32.33 32.29	34.08 32.13 31.52	34.25 32.38 31.76	34.61 33.21 33.22	35.20 33.61 33.62	34.57 33.43 34.02	34.80 33.95 33.94
Average	35.19	36.46	36.61	35.33	35.65	36.88	37.27	37.12	37.71

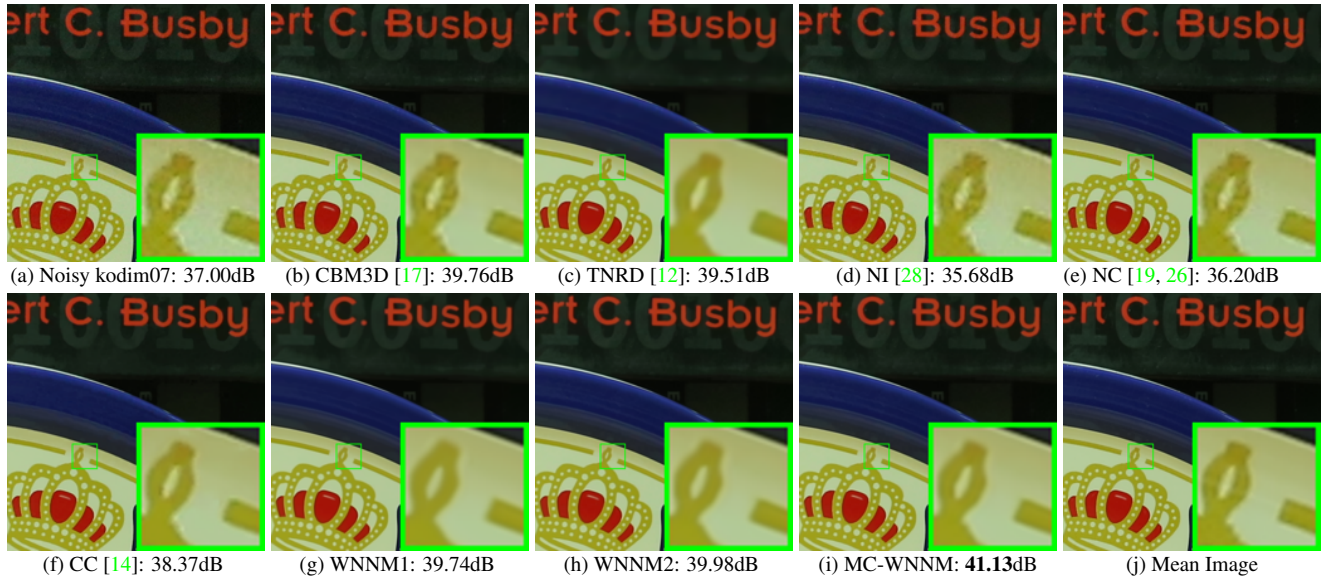


Figure 5. Denoised images of a region cropped from the real noisy image “Canon 5D Mark 3 ISO 3200 1” [14] by different methods. The images are better to be zoomed in on screen.

problem with two separable variables. We also studied the convergence property of the ADMM algorithm. Extensive experiments on synthetic and real color image denoising demonstrate that, the proposed MC-WNNM model outperforms the other competing denoising methods on both synthetic color noisy images as well as real-world noisy images. Introducing a weighting matrix to the traditional models for grayscale image denoising can boost the performance of traditional models on color image denoising tasks. We believe that this work can be extended in at least two directions. Firstly, the weighting matrix beyond the diag-

onal form, such as correlation form [31], may bring better performance on color image denoising. Secondly, the proposed MC-WNNM model can be further extended to deal with hyperspectral images, which may contain hundreds of channels (bands) with different noise structures in different channels.

References

- [1] A. Buades, B. Coll, and J. M. Morel. A non-local algorithm for image denoising. *IEEE Conference on Computer Vision*

- and Pattern Recognition (CVPR)*, pages 60–65, 2005. 1

[2] K. Dabov, A. Foi, V. Katkovnik, and K. Egiazarian. Image denoising by sparse 3-D transform-domain collaborative filtering. *IEEE Transactions on Image Processing*, 16(8):2080–2095, 2007. 1, 2

[3] M. Elad and M. Aharon. Image denoising via sparse and redundant representations over learned dictionaries. *IEEE Transactions on Image Processing*, 15(12):3736–3745, 2006.

[4] J. Mairal, F. Bach, J. Ponce, G. Sapiro, and A. Zisserman. Non-local sparse models for image restoration. *IEEE International Conference on Computer Vision (ICCV)*, pages 2272–2279, 2009.

[5] W. Dong, L. Zhang, G. Shi, and X. Li. Nonlocally centralized sparse representation for image restoration. *IEEE Transactions on Image Processing*, 22(4):1620–1630, 2013.

[6] J. Xu, L. Zhang, W. Zuo, D. Zhang, and X. Feng. Patch group based nonlocal self-similarity prior learning for image denoising. *IEEE International Conference on Computer Vision (ICCV)*, pages 244–252, 2015.

[7] S. Gu, L. Zhang, W. Zuo, and X. Feng. Weighted nuclear norm minimization with application to image denoising. *IEEE Conference on Computer Vision and Pattern Recognition (CVPR)*, pages 2862–2869, 2014. 1, 2, 5

[8] S. Roth and M. J. Black. Fields of experts. *International Journal of Computer Vision*, 82(2):205–229, 2009. 1

[9] D. Zoran and Y. Weiss. From learning models of natural image patches to whole image restoration. *IEEE International Conference on Computer Vision (ICCV)*, pages 479–486, 2011.

[10] H. C. Burger, C. J. Schuler, and S. Harmeling. Image denoising: Can plain neural networks compete with BM3D? *IEEE Conference on Computer Vision and Pattern Recognition (CVPR)*, pages 2392–2399, 2012. 5, 6, 7

[11] U. Schmidt and S. Roth. Shrinkage fields for effective image restoration. *IEEE Conference on Computer Vision and Pattern Recognition (CVPR)*, pages 2774–2781, June 2014.

[12] Y. Chen, W. Yu, and T. Pock. On learning optimized reaction diffusion processes for effective image restoration. *IEEE Conference on Computer Vision and Pattern Recognition (CVPR)*, pages 5261–5269, 2015. 1, 5, 6, 7, 8

[13] B. Leung, G. Jeon, and E. Dubois. Least-squares luma-chroma demultiplexing algorithm for bayer demosaicking. *IEEE Transactions on Image Processing*, 20(7):1885–1894, 2011. 1, 2

[14] S. Nam, Y. Hwang, Y. Matsushita, and S. J. Kim. A holistic approach to cross-channel image noise modeling and its application to image denoising. *IEEE Conference on Computer Vision and Pattern Recognition (CVPR)*, pages 1683–1691, 2016. 1, 2, 5, 6, 7, 8

[15] H. C. Karaimer and M. S. Brown. A software platform for manipulating the camera imaging pipeline. *European Conference on Computer Vision (ECCV)*, October 2016. 1

[16] Julien Mairal, Michael Elad, and Guillermo Sapiro. Sparse representation for color image restoration. *IEEE Transactions on Image Processing*, 17(1):53–69, 2008. 1, 2

[17] K. Dabov, A. Foi, V. Katkovnik, and K. Egiazarian. Color image denoising via sparse 3D collaborative filtering with grouping constraint in luminance-chrominance space. *IEEE International Conference on Image Processing (ICIP)*, pages 313–316, 2007. 1, 2, 5, 6, 7, 8

[18] C. Liu, R. Szeliski, S. Bing Kang, C. L. Zitnick, and W. T. Freeman. Automatic estimation and removal of noise from a single image. *IEEE Transactions on Pattern Analysis and Machine Intelligence*, 30(2):299–314, 2008. 1, 2

[19] M. Lebrun, M. Colom, and J.-M. Morel. Multiscale image blind denoising. *IEEE Transactions on Image Processing*, 24(10):3149–3161, 2015. 1, 2, 5, 6, 7, 8

[20] F. Zhu, G. Chen, and P.-A. Heng. From noise modeling to blind image denoising. *IEEE Conference on Computer Vision and Pattern Recognition (CVPR)*, June 2016. 1, 2

[21] S. Boyd, N. Parikh, E. Chu, B. Peleato, and J. Eckstein. Distributed optimization and statistical learning via the alternating direction method of multipliers. *Found. Trends Mach. Learn.*, 3(1):1–122, January 2011. 1

[22] C. Lu, C. Zhu, C. Xu, S. Yan, and Z. Lin. Generalized singular value thresholding. *AAAI*, 2015. 1

[23] J. Cai, E. J. Candès, and Z. Shen. A singular value thresholding algorithm for matrix completion. *SIAM Journal on Optimization*, 20(4):1956–1982, 2010. 2

[24] S. Gu, Q. Xie, D. Meng, W. Zuo, X. Feng, and L. Zhang. Weighted nuclear norm minimization and its applications to low level vision. *International Journal of Computer Vision*, pages 1–26, 2016. 2, 4, 5, 6

[25] C. Eckart and G. Young. The approximation of one matrix by another of lower rank. *Psychometrika*, 1(3):211–218, 1936. 2

[26] M. Lebrun, M. Colom, and J. M. Morel. The noise clinic: a blind image denoising algorithm. <http://www.ipol.im/pub/art/2015/125/>. Accessed 01 28, 2015. 2, 5, 6, 7, 8

[27] C. Kervrann, J. Boulanger, and P. Coupé. Bayesian non-local means filter, image redundancy and adaptive dictionaries for noise removal. *International Conference on Scale Space and Variational Methods in Computer Vision*, pages 520–532, 2007. 2

[28] Neatlab ABSoft. Neat Image. <https://neatvideo.com/home>. 2, 5, 6, 8

- 972 [29] X. Liu, M. Tanaka, and M. Okutomi. Single-image noise 1026
973 level estimation for blind denoising. *IEEE Transactions on 1027
974 Image Processing*, 22(12):5226–5237, 2013. 5 1028
975
976 [30] G. Chen, F. Zhu, and A. H. Pheng. An efficient statistical 1029
977 method for image noise level estimation. *IEEE International 1030
978 Conference on Computer Vision (ICCV)*, December 2015. 5, 1031
979 6 1032
980 [31] N. J. Higham. Computing the nearest correlation matrixa 1033
981 problem from finance. *IMA Journal of Numerical Analysis*, 1034
982 22(3):329, 2002. 8 1035
983
984
985
986
987
988
989
990
991
992
993
994
995
996
997
998
999
1000
1001
1002
1003
1004
1005
1006
1007
1008
1009
1010
1011
1012
1013
1014
1015
1016
1017
1018
1019
1020
1021
1022
1023
1024
1025